Journal of Power Sources 269 (2014) 962–974

Contents lists available at ScienceDirect

Journal of Power Sources

journal homepage: www.elsevier.com/locate/jpowsour

Practical thermodynamic quantities for aqueous vanadium- and iron-based flow batteries

Nicholas S. Hudak*

Advanced Power Sources Research and Development, Sandia National Laboratories, P.O. Box 5800 MS 0613, Albuquerque, NM 87185-0613, USA

HIGHLIGHTS

- Experimentally measured thermodynamic quantities for flow batteries are presented.
- Measured thermodynamic quantities differ from published standard values.
- Cell reaction entropy as a function of state-of-charge follows the Nernst Equation.
- Practical thermodynamic quantities can be used in flow battery modeling and design.
- Non-isothermal flow cell cycling exhibits improved voltage efficiency in some cases.

GRAPHICAL ABSTRACT

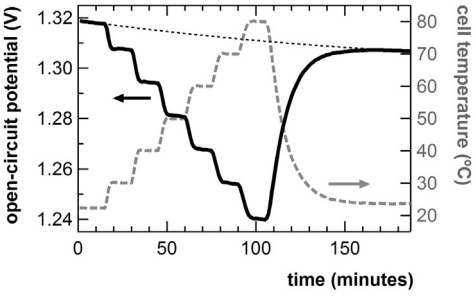

ARTICLE INFO

Article history:
Received 24 September 2013
Received in revised form
9 November 2013
Accepted 18 December 2013
Available online 31 December 2013

Keywords:
Flow battery
Thermodynamics
Entropy
Formal potential
Nernst Equation
Non-isothermal

ABSTRACT

A simple method for experimentally determining thermodynamic quantities for flow battery cell reactions is presented. Equilibrium cell potentials, temperature derivatives of cell potential (dE/dT), Gibbs free energies, and entropies are reported here for all-vanadium, iron–vanadium, and iron–chromium flow cells with state-of-the-art solution compositions. Proof is given that *formal potentials* and *formal temperature coefficients* can be used with modified forms of the Nernst Equation to quantify the thermodynamics of flow cell reactions as a function of state-of-charge. Such empirical quantities can be used in thermo-electrochemical models of flow batteries at the cell or system level. In most cases, the thermodynamic quantities measured here are significantly different from standard values reported and used previously in the literature. The data reported here are also useful in the selection of operating temperatures for flow battery systems. Because higher temperatures correspond to lower equilibrium cell potentials for the battery chemistries studied here, it can be beneficial to charge a cell at higher temperature and discharge at lower temperature. Proof-of-concept of improved voltage efficiency with the use of such non-isothermal cycling is given for the all-vanadium redox flow battery, and the effect is shown to be more pronounced at lower current densities.

1. Introduction

As worldwide demand for electricity continues to rise, there is a need for increased utilization of energy storage in the electrical grid [1]. The use of energy storage will improve grid reliability and efficiency, and it will enable further incorporation of renewable, intermittent energy sources such as wind and solar power [1,2]. The redox flow battery (RFB) is one of several energy storage technologies that are appropriate for the utility scale. Advantages of RFBs over other types of energy storage include the possibility for millisecond response times, the direct conversion from chemical to

* Tel.: +1 505 844 2171; fax: +1 505 844 6972.
E-mail address: nhudak@sandia.gov.

0378-7753/$ – see front matter © 2014 Elsevier B.V. All rights reserved.
http://dx.doi.org/10.1016/j.jpowsour.2013.12.089

electrical energy, the ability to be sited anywhere, and the ability for energy content and power output to be scaled independently [3,4]. Accordingly, there has been a large amount of research in RFBs in recent years. The work has mainly been aimed at improving the cycling stability and energy efficiency of established cell chemistries and exploring new cell chemistries with potentially higher specific energies [5].

One approach to understanding and improving RFB performance is to develop cell-level models that incorporate electrochemistry, mass transport, reaction kinetics, and thermodynamics. Such models have been developed, with varying degrees of complexity, and compared to experimental results for all-vanadium [6–13], iron–vanadium [14], and iron–chromium [15] flow batteries. All such models of electrochemical systems must account for the thermodynamics of the cell reaction or individual electrode reactions in order to accurately predict the observed, measurable quantities of cell potential and heat output. The Gibbs free energy (ΔG) of the cell is present in even the simplest electrochemical models; it represents the maximum net amount of work obtainable from the cell and is proportional to cell potential (E) [16]. Thermo-electrochemical models of battery cells (those that incorporate heat output or consumption and do not assume constant temperature) must also account for the entropy (ΔS) of the cell [6,17,18]. This quantity represents the heat output or consumption of the cell under reversible conditions and is proportional to dE/dT, the partial derivative of cell potential with respect to temperature (also called the "temperature coefficient" [19]). (Note: Although temperature coefficients are partial derivatives, they are expressed here and in some previous references as dE/dT rather than $\partial E/\partial T$, for the sake of simplicity.)

In almost all cases, the thermodynamic quantities that were "plugged into" the models cited above were from unverified and varied sources. In many cases, the original sources for the reported values are difficult to identify, and various references reported conflicting values for the same species or electrode reactions. This is especially true for the entropy values, which have in some cases been estimated by "daisy-chaining" the experimental or calculated results from various studies conducted under different conditions [20]. Furthermore, the quantities used in the above-cited models were usually *standard* thermodynamic quantities, which assume standard conditions and unit activity for all dissolved species. The use of standard potentials (E^0), standard Gibbs free energies (ΔG^0), and standard entropies (ΔS^0) to model the electrode reactions or cell reactions of flow batteries is unlikely to produce accurate results. This is because the high concentrations of active redox species and supporting electrolytes that are typically used in flow batteries may result in species activities that are far from unity. Indeed, measured cell potentials of vanadium redox flow batteries (VRFB) have differed by as much as 140 mV from simulated values that were obtained by using the reported standard cell potential [7,9,12,13,21,22]. In one case, this discrepancy was accounted for by incorporating the solution's proton activity and the membrane's Donnan potential into the expression for cell potential [23]. However, the two effects could not be measured and verified separately, and the analysis was based on the assumption that previously published standard potential values were accurate. Several models arbitrarily applied a correction factor to the cell potential when the modeled potential curves did not match the experimental ones [9,12–14]. Thus, the equilibrium cell potential (along with its associated ΔG) has effectively become an additional fitted parameter rather than an independently determined value.

Presented here are the formal potential values ($E^{0\prime}$), determined experimentally, for the cell reactions of aqueous all-vanadium, iron–vanadium, and iron–chromium flow batteries with typical concentrations of active materials and supporting electrolytes. Use of the *formal potential* [16] for a specific cell composition rather than the standard potential of the cell reaction avoids the need for activity coefficients or arbitrary corrections and provides practical thermodynamic values that can be used in cell- or system-level models. Additionally, the concept of a *formal temperature coefficient* ($dE^{0\prime}/dT$) is introduced here and measured for the three flow battery chemistries. As shown here and verified experimentally, the derivative of the Nernst Equation with respect to temperature can be used with the formal temperature coefficient to determine the temperature coefficient at any state-of-charge. The formal potential and temperature coefficient values for a given cell chemistry can be easily converted to the Gibbs free energy and entropy, respectively, for use in thermo-electrochemical models. While these values are specific to the flow battery chemistry and supporting electrolyte with which they are measured, the experimental method is simple and can be easily replicated to determine thermodynamic values for other flow battery compositions. Furthermore, the temperature coefficient values can be used for a more informed design of flow battery systems, specifically in the selection of operating temperature during cell charge and discharge. An example of such design, in which operation of charge and discharge at different temperatures results in improved efficiency relative to isothermal operation, is given with experimental verification.

2. Experimental methods

2.1. Materials

Vanadium(IV) oxide sulfate ($VOSO_4$) hydrate and chromium(III) chloride hexahydrate were used as received from Alfa Aesar. Iron(II) chloride tetrahydrate and vanadium(III) chloride were used as received from Sigma–Aldrich. An aqueous solution consisting of ~2 M $VOSO_4$ and 6 M HCl was prepared and used for the all-vanadium redox flow cells. This solution is referred to as a "sulfate–chloride mixed electrolyte" and is the state-of-the-art for VRFB [24]. This type of solution was chosen for the present study because it has an expanded temperature range and increased solubility compared to chloride-free VRFB solutions. An aqueous solution of 1.25 M $FeCl_2$, 1.25 M VCl_3, and 2.3 M HCl was prepared for the iron–vanadium (Fe–V) flow cells [25]. An aqueous solution of 1.25 M $FeCl_2$, 1.25 M $CrCl_3$, and 2.3 M HCl was prepared for the iron–chromium (Fe–Cr) flow cells [26]. The electrolyte solutions for Fe–V and Fe–Cr cells are called "mixed reactant solutions" because both metal ions are present in the same solution, which is used on both the positive and negative sides of the cell to prevent reactant crossover through the membrane.

Nafion 117 membranes (Ion Power) were used as received and stored in DI water at room temperature for at least 24 h prior to cell assembly [27]. Neosepta AMX anion-exchange membranes (ASTOM Corporation) were used as received and stored in 3 wt% NaCl, as directed by the manufacturer. Sigracell GFD2.5 carbon felt (SGL Carbon) was placed under O_2 plasma for 10 min using a Harrick plasma cleaner immediately prior to use in flow cells [28]. This "pre-treatment" process rendered the carbon felt hydrophilic.

2.2. Flow cell setup

Flow cell experiments were performed with an "acid cell" test fixture from Fuel Cell Technologies (Albuquerque, New Mexico, USA). The current collectors in this fixture were made of Poco graphite blocks with machined serpentine flow fields and 5-cm^2 active area. Pre-treated carbon felt was used as the electrode on each side of the cell, and Nafion 117 or Neosepta AMX was used as the electrolyte membrane. Polytetrafluoroethylene (PTFE) sheets and PTFE-coated fiberglass fabric were used as gaskets, and the

total gasket thickness on each side was approximately 80% of the carbon felt thickness. Liquid electrolyte flow was directed into the graphite blocks via fluoropolymer tubing and tube fittings. The flow was controlled with a peristaltic pump with Viton tubing attached to the fluoropolymer fittings. The external electrolyte reservoirs consisted of glass vials with PTFE-lined caps. During cell operation, the reservoirs were supplied with a constant flow of argon gas to prevent oxidation of active materials. Cell temperature was controlled using an Omega CSC232 temperature controller connected to a thermocouple and cartridge heaters embedded into the cell hardware. The lowest attainable cell temperature was 22 °C.

2.3. Electrochemical testing

Electrochemical testing of flow cells was performed with a PAR 273A potentiostat/galvanostat. Cell charging, discharging, and cycling were performed in galvanostatic mode at 50 mA cm^{-2} (250 mA) unless otherwise specified. Liquid flow on both sides of the cell was 10 mL min^{-1} during electrochemical testing unless otherwise specified.

2.4. Measurement of temperature coefficient (dE/dT)

The temperature coefficient (partial derivative of open-circuit cell potential with respect to temperature) was measured by holding the cell temperature at 22 °C, incrementally increasing it by ~10 °C steps to 80 °C, and lowering it back down to room temperature. Each temperature step lasted 15 min. Open-circuit cell potential (OCP) was measured at 1-min intervals during this procedure with a Fluke 8845A digital multimeter, which has 6.5-digit precision. The flow rate on both sides of the cell was maintained at 0.1 mL min^{-1} during dE/dT measurement. In cases where an electrochemical charge or discharge preceded dE/dT measurement, the cell was allowed to equilibrate at open circuit for 2 h at 22 °C and 0.1 mL min^{-1} before raising the temperature. Temperature and cell OCP data for a typical dE/dT measurement is shown in Fig. 1(a). As shown, there is a slight drift downward in OCP, regardless of cell temperature. This slow self-discharge is likely due to active redox components diffusing through the membrane. To correct for this drift, a baseline potential profile was determined for each data set by performing a 2nd-order polynomial fit to the OCP vs. time data at 22–24 °C (room temperature). The resultant baseline potential profile is also shown in Fig. 1(a). The baseline-corrected potential at each point in time was calculated by subtracting the room-temperature baseline potential from the measured potential at each temperature and adding the 22 °C potential value (taken just before the first temperature increase). The baseline-corrected OCP profile for the sample cell is shown in Fig. 1(b). The corrected OCP at each temperature step (taken just before the subsequent temperature increase) was plotted vs. temperature, as shown in Fig. 1(c). A least-squares linear fit of these data was performed, the slope of which is the dE/dT value.

For the Fe–Cr cells, only the three data points from 22–40 °C were used in the linear fit dE/dT because the voltage drift at higher temperatures was too high to produce a linear response, even after the baseline correction was applied. Thus, the room-temperature baseline correction in these cases could not correct for the faster voltage drift at higher temperatures. This is likely due to self-discharge of the cell, which is more significant at higher temperatures. Although Neosepta AMX is an anion-exchange membrane, it is likely that the iron and chromium cations pass through the membrane at these higher temperatures, resulting in prohibitively unstable voltage. The membrane has not been extensively tested in flow batteries and is not rated for use at the higher temperatures. A similar situation was encountered with Nafion-loaded VRFB cells at OCP above 1.42 V or below 1.26 V. In these cases, only the data

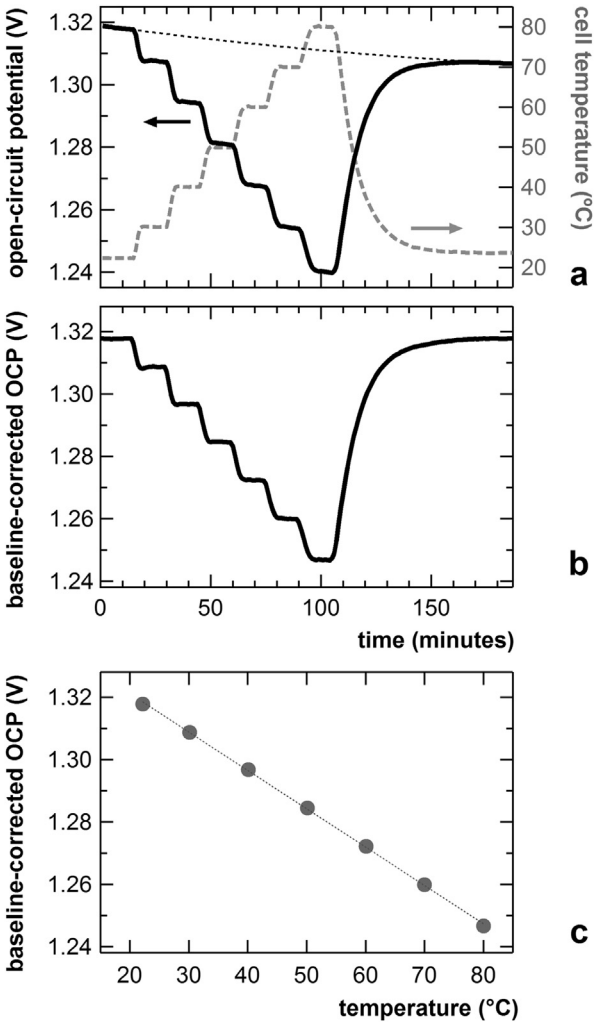

Fig. 1. Data and analysis for a typical dE/dT measurement (VRFB cell at 13.3% state-of-charge). (a) Measured cell temperature and open-circuit cell potential (OCP) vs. time during incremental changes in set temperature. Also shown is the baseline voltage profile (dotted black line), determined by a 2nd-order polynomial fit of the 22 °C OCP vs. time data. (b) Baseline-corrected OCP vs. time. (c) Baseline-corrected OCP (markers) vs. temperature with least-squares linear fit (dotted line).

points from 22–50 °C were used in the linear fit. This is a somewhat expected result as Nafion is a cation-exchange membrane, allowing the various vanadium cations to pass through it. The measured dE/dT values of the cells in question may be valid at higher temperatures given that a linear OCP-temperature response was observed over the range 22–80 °C in other cells. However, this cannot be stated with certainty because of inability to measure reliable, constant dE/dT values for the cells in question at higher temperatures using this method.

3. Results and discussion

3.1. All-vanadium (VRFB) cells

3.1.1. Cell reactions and published thermodynamic data

The half-cell reaction on the negative electrode side of a VRFB is:

$$V^{2+} \leftrightarrow V^{3+} + e^{-} \quad (1)$$

The forward direction of this reaction, and all subsequent reactions as expressed in this text, occurs during cell discharge.

Table 1
Published thermodynamic quantities for the negative electrode reaction of the all-vanadium redox flow battery (VRFB). ΔG^0 values are in kJ mol^{-1} and E^0 values are in volts vs. SHE (standard hydrogen electrode).

Source	Year	ΔG_f^0 of V^{3+}	ΔG_f^0 of V^{2+}	ΔG^0 of half-cell reaction	E^0 of half-cell reaction	Remarks
Jones and Colvin [33]	1944	N/A	N/A	24.6	−0.255	Experimentally determined
Pourbaix book [31]	1966	−251.4	−227	24.6	−0.255	Compiled from various references
Hill et al. review [20]	1971	−242	−218	24	−0.249	Calculated from various references
Post and Robins [30]	1976	−251	−227	24.7	−0.256	Compiled from various references
Bard et al. book [29]	1985	−251.3	−218	33.3	−0.345	Compiled from various references
Bratsch tables [32]	1989	N/A	N/A	24.6	−0.255	Compiled from various references

Table 1 contains the standard Gibbs free energy of formation (ΔG_f^0) for the two vanadium species, culled from various publications [20,29–31], along with the ΔG^0 and E^0 of the half-cell reduction reaction calculated from these values. In some cases, ΔG^0 or E^0 of this half-cell reaction were reported directly [32,33]. As is evident in the table, some of the reported values from comprehensive tables of thermodynamic data have been taken directly from previous references in the table. This is also true for subsequent tables of published data given here. While there is general agreement among these ΔG^0 values, with some slight variation, Table 2 shows that there is no agreement over the corresponding ΔS^0 and dE^0/dT values. Most values were estimated by "daisy-chaining" values from other reactions [20,29] or are from unspecified original sources [6].

The half-cell reaction on the positive electrode side of a VRFB is:

$$VO_2^+ + 2H^+ + e^- \leftrightarrow VO^{2+} + H_2O \quad (2)$$

The standard Gibbs free energy of formation (ΔG_f^0) for these two vanadium species, along with the ΔG^0 and E^0 values for reduction in the half-cell, are given in Table 3 [20,29,31,32,34–37]. Calculation of the half-cell ΔG^0 accounts for the ΔG_f^0 of the H_2O molecule involved in the reaction (−237.14 kJ mol^{-1} as reported in Dean and Lange [38]). As shown, there is good agreement among the values in Table 3. In contrast, the entropy values for Reaction 2, shown in Table 4, are grouped around two significantly different values, −87 J mol^{-1} K^{-1} [32,34,35] and −20 J mol^{-1} K^{-1} [20,29,36,37]. Evidently, the former values were calculated without accounting for the S^0 value of H_2O, which is 69.95 J mol^{-1} K^{-1} [38]. Thus, it can safely be assumed that entropy values around −20 J mol^{-1} K^{-1} are more accurate. However, there is little experimental evidence to support this or to provide a more precise value.

The full-cell VRFB reaction is obtained by combining Equations (1) and (2):

$$V^{2+} + VO_2^+ + 2H^+ \leftrightarrow V^{3+} + VO^{2+} + H_2O \quad (3)$$

The standard thermodynamic values of the full cell can be obtained by subtracting the standard values of the negative side from those of the positive side. The standard thermodynamic values for the full VRFB cell from various published sources are shown in Table 5. The reported standard cell potential E^0 varies from 1.25 V to 1.34 V, and reported dE^0/dT values are either −1.2 or −2.4 mV K^{-1}. There is only one known previous study in which an experimental dE/dT was given for a VRFB [21]. The authors claimed that dE/dT was measured at a state-of-charge corresponding to the standard cell potential, but the resultant value of −1.62 mV K^{-1} does not agree with either of the previously reported values.

The large amount of variation in standard thermodynamic values that have been reported for the VRFB half-cell and full-cell reactions underscores the need for empirical values that are measured with relevant cell compositions. Use of the reported values for standard Gibbs free energy and entropy, along with the corresponding OCP and temperature coefficient values, in flow battery models is not sufficient to obtain accurate results. As mentioned above, several flow battery models arbitrarily applied a correction factor to the cell potential when the modeled curves did not match the experimental ones [9,12–14]. In one case, a non-isothermal model of a flow battery used inconsistent values for ΔS and dE/dT [6] because the values were obtained from multiple references [29,32] that reported conflicting values. As demonstrated below, a simpler and more straightforward approach is to use empirical formal potentials to obtain the various thermodynamic quantities for specific cell chemistries.

3.1.2. Nernst Equation with formal potential

The Nernst Equation [16] can be applied to the full-cell VRFB reaction (Equation (3), for which $n = 1$ equiv mol^{-1}) to obtain an expression for the equilibrium cell potential, or OCP (the potential at zero net current flow):

$$E = E^0 + \frac{RT}{F}\ln\left(\frac{a_{V^{2+}} \cdot a_{VO_2^+} \cdot (a_{H^+})^2}{a_{V^{3+}} \cdot a_{VO^{2+}}}\right) \quad (4)$$

where E is the measured OCP in units of volts, R is the universal gas constant (8.3145 J mol^{-1} K^{-1}), T is temperature in Kelvin, F is the Faraday constant (96485 C equiv^{-1}), and a_k is the activity of species k in solution (unitless). The solutions are assumed to exhibit ideal behavior despite the ionic nature of the active species. Thus, each activity value can be expressed as a function of activity coefficient γ (unitless), species concentration (bracketed terms in mol L^{-1}), and standard concentration c^0 (constant value in mol L^{-1}): $a_k = \gamma_k \cdot [k]/c^0$. The activity coefficients are assumed to be constant over the full range of state-of-charge. A separate logarithmic term comprising the constants (activity coefficients and standard

Table 2
Published thermodynamic quantities for the negative electrode reaction of the VRFB. S^0 values are in J mol^{-1} K^{-1} and dE^0/dT values are in mV K^{-1}. Values in parentheses are estimated, as stated by the source author(s).

Source	Year	S^0 of V^{3+}	S^0 of V^{2+}	ΔS^0 of half-cell reaction	dE^0/dT of half-cell reaction	Remarks
Jones and Colvin [33]	1944	N/A	N/A	39	0.40	Experimentally determined from data at 0 °C and 25 °C
Hill et al. review [20]	1971	(−230)	(−130)	(100)	(1.0)	Calculated from various references
Bard et al. book [29]	1985	(−230)	(−130)	(100)	(1.0)	From Hill 1971 reference
Bratsch tables [32]	1989	N/A	N/A	(140)	(1.5)	Compiled from various references

Table 3
Published thermodynamic quantities for the positive electrode reaction of the VRFB. ΔG^0 values are in kJ mol^{-1} and E^0 values are in volts vs. SHE (standard hydrogen electrode).

Source	Year	ΔG_f^0 of VO_2^+	ΔG_f^0 of VO^{2+}	ΔG^0 of half-cell reaction	E^0 of half-cell reaction	Remarks
Coryell and Carpenter articles [34,35]	1933–1934	N/A	N/A	−96.45	0.9996	Experimentally determined
LaSalle and Cobble [36]	1955	−598	−460	−99.1	1.02	Combination of experiment and previous references
Pourbaix book [31]	1966	−596.4	−456	−96.8	1.004	Compiled from various references
Hill et al. review [20]	1971	−587.4	−446.8	−96.54	1.000	Calculated from various references
Wagman et al. tables [37]	1982	−587.0	−446.4	−96.54	1.000	Comprehensive NBS (NIST) tables
Bard et al. book [29]	1985	−587.0	−446.4	−96.54	1.000	From Wagman et al. tables
Bratsch tables [32]	1989	N/A	N/A	−96.58	1.001	Compiled from various references

concentration) is combined with the standard potential to form the formal potential $E^{0\prime}$, thus allowing the expression of cell OCP in terms of reactant concentrations:

$$E = E^{0\prime} + \frac{RT}{F}\ln\left(\frac{[V^{2+}]\cdot[VO_2^+]\cdot[H^+]^2}{[V^{3+}]\cdot[VO^{2+}]}\right) \quad (5)$$

Given the stoichiometry in Reaction (3), and assuming equal amounts and concentrations of total vanadium species on both sides the full cell, this expression can be simplified to yield:

$$E = E^{0\prime} + \frac{2RT}{F}\ln\left(\frac{[V^{2+}]\cdot[H^+]}{[V^{3+}]}\right) \quad (6)$$

The concentrations of various species in Equation (6) can be related to the state-of-charge (SOC) of the VRFB as follows. The SOC can be quantified as $[V^{2+}]/([V^{2+}] + [V^{3+}])$; thus, the ratio $[V^{2+}]/[V^{3+}]$ is equivalent to $X/(1 - X)$ where X is the SOC. Using the stoichiometry in Reaction (3), the proton concentration $[H^+]$ at any SOC is equivalent to $([H^+]_{x=0} + 2X\cdot[V^{3+}]_{x=0})$. In this case, the H^+ and V^{3+} concentrations of a fully discharged cell are 6 M and 2 M, respectively. Thus, the full expression for cell OCP as a function of SOC (X) is as follows:

$$E = E^{0\prime} + \frac{2RT}{F}\ln\left(\frac{6X + 4X^2}{1 - X}\right) \quad (7)$$

The formal potential $E^{0\prime}$ can be determined by measuring the OCP of the cell at $X = 13.3\%$. This is the SOC at which the logarithmic term in Equation (7) equals zero. This SOC and the logarithmic term in Equation (7) are unique to the total concentration of active redox species and the concentration of dissociated protons in the VRFB (6 M and 2 M, respectively, in this case). Alternate versions of Equation (7) for other cell compositions can be easily determined.

The formal potential $E^{0\prime}$ at 22 °C of the VRFB chemistry used in this study was determined by measuring cell OCP at 13.3% SOC as follows. The cell was prepared with 30 mL of $VOSO_4$ solution on the positive electrode side and 15 mL of the same solution on the negative electrode side. The cell was fully charged to an upper voltage limit of 1.9 V, which results in a vanadium oxidation state of +5 on the positive side and +2 on the negative side. A volume of 15 mL was immediately removed from the positive electrolyte reservoir to obtain a balanced cell. The cell was fully discharged, to 0.5 V, and allowed to sit at open circuit overnight for the H^+ concentration on both sides to equilibrate back to 6 M. The cell was fully charged again, and a 1.60-mL aliquot of "charged" solution was collected on each side and stored under argon. After another full discharge, 10.4 mL of "discharged" solution was collected on each side and thoroughly mixed with the corresponding 1.60-mL "charged" aliquot. The cell was rinsed by pumping DI water through both sides, and the 12-mL mixtures were pumped through each side to obtain a cell at 13.3% SOC. The OCP was immediately measured with a digital multimeter, and this value was taken as $E^{0\prime}$. The resultant value was $E^{0\prime} = 1.32$ V, which was confirmed to three significant figures in a duplicate experiment (i.e. the precision was ±0.00 V). The average E value is calculated by integrating Equation (7) over the range $\{0 \le X \le 1\}$. This results in a value $E_{avg} = 1.42$ V and occurs at $X = 0.498$.

The partial molar Gibbs free energy ($\Delta\overline{G}$) of the cell reaction at a particular SOC can be calculated using the measured $E^{0\prime}$ value with Equation (7) and the well-known relationship $\Delta\overline{G} = -nFE$ [16,39,40]. This yields the following expression:

$$\Delta\overline{G} = -FE^{0\prime} - 2RT\ln\left(\frac{6X + 4X^2}{1 - X}\right) \quad (8)$$

The Gibbs free energy of the cell over a full charge or discharge is equal to the integral of $\Delta\overline{G}$ over the range $\{0 \le X \le 1\}$. This calculation is equivalent to taking the average cell potential E_{avg} and multiplying it by the Faraday constant or to plugging the value $X = 0.498$ into Equation (8). The result is $\Delta G = -138$ kJ mol^{-1}. As shown in Table 5, this ΔG value differs significantly from previously reported standard values that were used in VRFB models.

Use of Equation (7) to calculate the cell potential as a function of formal potential and state-of-charge was verified by comparing the calculated values to measured charge–discharge curves. The calculated potential at 22 °C using $E^{0\prime} = 1.32$ V with Equation (7) is shown in Fig. 2(a) as a function of SOC. This is compared to an

Table 4
Published thermodynamic quantities for the positive electrode reaction of the VRFB. S^0 values are in J mol^{-1} K^{-1} and dE^0/dT values are in mV K^{-1}.

Source	Year	S^0 of VO_2^+	S^0 of VO^{2+}	ΔS^0 of half-cell reaction	dE^0/dT of half-cell reaction	Remarks
Coryell and Carpenter articles [34,35]	1933–1934	N/A	N/A	−86.6	−0.898	
LaSalle and Cobble [36]	1955	−23	−110	−17	−0.18	Combination of experiment and previous references
Hill et al. review [20]	1971	−41	−130	−19	−0.20	Calculated from various references
Wagman et al. tables [37]	1982	−42.3	−133.9	−21.6	−0.224	Comprehensive NBS (NIST) tables
Bard et al. book [29]	1985	−42.3	−133.9	−21.6	−0.224	From Wagman et al. tables
Bratsch tables [32]	1989	N/A	N/A	−86.9	−0.901	Compiled from various references

Table 5
Thermodynamic quantities for the VRFB cell reaction.

Source	Year	ΔG of cell reaction (kJ mol^{-1})	E of cell (V)	ΔS of cell reaction (J mol^{-1} K^{-1})	dE/dT of cell (mV K^{-1})	Remarks
Pourbaix book [31]	1966	−121	1.26	N/A	N/A	Standard values
Hill et al. review [20]	1971	−120	1.25	−120	−1.2	Standard values
Bard et al. book [29]	1985	−130	1.34	−120	−1.2	Standard values
Bratsch tables [32]	1989	−121	1.26	−230	−2.4	Standard values
Heintz and Illenberger [21]	1998	−119.8	1.242	−156	−1.62	Experimental results based on calorimetry and dE/dT measurement
This work	2013	−138	1.32	−83.3	−1.22	Formal potential (22 °C) and dE/dT (22–80 °C) measured at 13.3% SOC

experimental charge–discharge curve measured at 50 mA cm^{-2} and 22 °C with a Nafion 117 membrane. A formal potential for 60 °C, measured as 1.27 V, was used similarly to calculate an OCP vs. SOC curve and compared to experimental results, as shown in Fig. 2(b). At both temperatures, the calculated OCP curve lies approximately midway between the charge and discharge curves. The average potential of the measured charge and discharge curves is 1.43 V, which is close to the value $E_{avg} = 1.42$ V calculated above. These results confirm the use of the Nernst Equation with temperature- and composition-specific formal potentials to simulate cell potential as a function of state-of-charge. Conversely, the state-of-charge of a VRFB cell can be calculated from a measured OCP using Equation (7). It is also worth noting that a simpler form of Equation (7), in which the H^+ concentration is ignored, can be used to produce a similar potential curve. This form of the Nernst Equation is same as Equation (16), described below for Fe–V cells. In that case, $E^{0\prime}$ is measured at $X = 0.500$, and this potential is also the average over the entire range of state-of-charge. Calculated potential curves

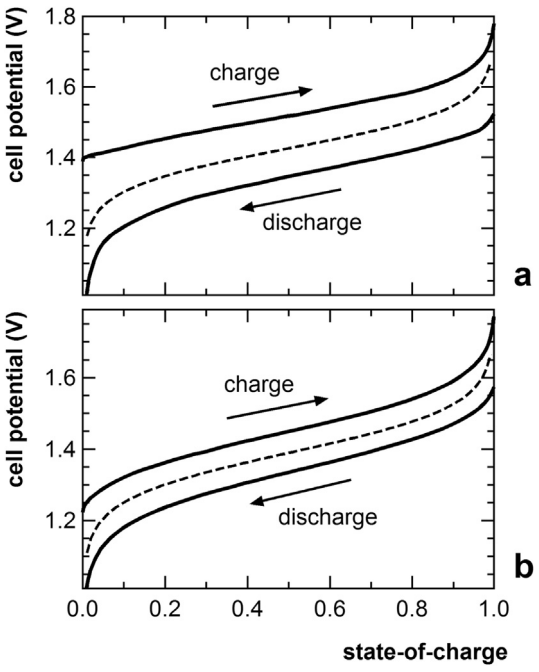

Fig. 2. Measured galvanostatic charge–discharge potential (solid lines) compared to calculated OCP (dashed lines) for the VRFB cell. (a) 22 °C, at which $E^{0\prime} = 1.32$ V. (b) 60 °C, at which $E^{0\prime} = 1.27$ V. SOC for the experimental charge curves was determined by dividing charge time by total charge time. SOC for the experimental discharge curves was determined by dividing discharge time by total discharge time and subtracting the quotient from 1. OCP was calculated using the Nernst Equation (Equation (7)) with the measured formal potential $E^{0\prime}$.

for the VRFB at 22 °C and 60 °C using this simpler form differed from those using Equation (7) by less than 17 mV over the range $\{0 \le X \le 1\}$. Because of the small difference, some modelers may choose to use the simpler form of the Nernst Equation and measure the formal potential at 50% SOC.

3.1.3. Temperature coefficient and entropy values

An expression for the cell temperature coefficient dE/dT can be obtained by taking the derivative of Equation (7) with respect to temperature:

$$\frac{dE}{dT} = \frac{dE^{0\prime}}{dT} + \frac{2R}{F}\ln\left(\frac{6X + 4X^2}{1 - X}\right) \tag{9}$$

where dE/dT is in units of volts K^{-1}. Thus, the concept of the formal temperature coefficient (d$E^{0\prime}$/dT) is introduced and is measured at $X = 0.133$ for this VRFB composition, similar to the formal potential. As shown in Fig. 1(c), the cell OCP (corrected for baseline drift) has a linear relationship with temperature over the range 22–80 °C. Thus, d$E^{0\prime}$/dT for this system is constant. This experiment was performed in duplicate with two separately prepared cells, and the average of the two measurements was d$E^{0\prime}$/d$T = -1.22 \pm 0.02$ mV K^{-1}. As shown in Table 5, this value is equal to some of the previously published standard values, dE^0/d$T = -1.2$ mV K^{-1} [20,29], which suggests that this VRFB composition at 13.3% SOC is close to a standard state.

The calculated average dE/dT value over the full range of state-of-charge occurs at $X = 0.498$ and is equal to −0.863 mV K^{-1}. This value is significantly different from the only other measured dE/dT value for a VRFB cell, which was −1.62 mV K^{-1} at 20% SOC [21]. One possible explanation for the discrepancy is that the previous study did not apply a baseline correction, as was done in the present study. A decreasing OCP baseline, which usually occurs in VRFB cells with cation-exchange membranes, would result in measured dE/dT values that are artificially low (i.e. in this case, more highly negative than the actual values). Another explanation for the discrepancy is the difference in vanadium concentration, H^+ concentration from the supporting electrolyte, and composition of the supporting electrolyte (Cl^- vs. SO_4^-) between this and the previous study. Such differences would likely result in different activity coefficients, and this further stresses the need for empirical thermodynamic values to be obtained for specific flow battery compositions.

The partial molar entropy of the cell reaction ($\Delta\bar{S}$) at a particular SOC can be calculated by using Equation (9) with the well-known relationship $\Delta\bar{S} = nF(dE/dT)$ [16,39,40]. This results in the following expression:

$$\Delta\bar{S} = F\frac{dE^{0\prime}}{dT} + 2R\ln\left(\frac{6X + 4X^2}{1 - X}\right) \tag{10}$$

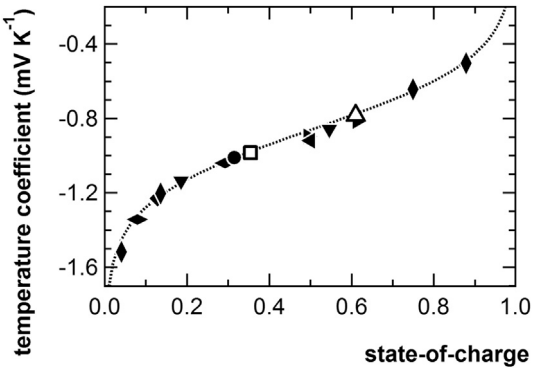

Fig. 3. Measured dE/dT (markers) compared to calculated dE/dT (line) as a function of state-of-charge X for the VRFB. The calculation was performed using Equation (9) (temperature derivative of the Nernst Equation) and the formal temperature coefficient, $dE^{0\prime}/dT = -1.22$ mV K^{-1}. The X value for each experimental dE/dT point was calculated using Equation (7) with the measured OCP at 22 °C and the formal potential at 22 °C ($E^{0\prime} = 1.32$ V). Different marker shapes correspond to separately prepared cells. Filled markers correspond to cells using Nafion 117 as membrane, and hollow markers correspond to cells using Neosepta AMX as membrane. There are 15 data points total, taken from 9 separately prepared cells.

The entropy of the cell over a full charge or discharge is equal to the integral of $\Delta\bar{S}$ over the range $\{0 \le X \le 1\}$. This calculation is equivalent to plugging the value $X = 0.498$, the SOC at which the average potential occurs, into Equation (10). The result is $\Delta S = -83.3$ J mol^{-1} K^{-1}, which is significantly different from previously published standard values as shown in Table 5.

In order to confirm the validity of Equation (9) and the concept of a formal temperature coefficient, dE/dT values were measured in VRFB cells at various states-of-charge. The SOC was varied by charging or discharging a cell for an arbitrary amount of time. The state-of-charge in each case was obtained by using the measured OCP at 22 °C in Equation (7) and solving for X. The measured data were compared to the dE/dT vs. X curve calculated using $dE^{0\prime}/dT = -1.22$ mV K^{-1} with Equation (9). The comparison is shown in Fig. 3, in which there is good agreement between measured and calculated values. This proves that the derivative of the Nernst Equation, as expressed in Equation (9), is valid for the VRFB. Fig. 3 also shows good repeatability of the measurements, as the data were gathered from nine separately prepared cells, using either Nafion 117 or Neosepta AMX as membrane.

Because the Nernst Equation has been validated above for relating state-of-charge, cell potential, and temperature coefficient, a combined expression for calculating cell OCP as a function of temperature and SOC (X) can be used for the given temperature range 22–80 °C:

$$E(T,X) = E^{0\prime}\Big|_{22\ ^\circ\mathrm{C}} + (T - 295\ K)\frac{dE^{0\prime}}{dT} + \frac{2RT}{F}\ln\left(\frac{6X + 4X^2}{1 - X}\right) \quad (11)$$

3.2. Iron–vanadium (Fe–V) cells

3.2.1. Cell reactions and published thermodynamic data

The half-cell reaction on the negative electrode side of the Fe–V flow battery is the same as that of the VRFB, given in Equation (1) above. The half-cell reaction on the positive side of the Fe–V flow battery is:

$$Fe^{3+} + e^- \leftrightarrow Fe^{2+} \quad (12)$$

Table 6 contains the standard Gibbs free energy of formation (ΔG_f^0) for these two oxidation states of iron in aqueous solution, culled from various publications [29,31,32,37,41,42]. The ΔG^0 and E^0 of the half-cell reaction calculated from these values are also given in Table 6. There is general agreement among the values for the half-cell reaction, some of which are from different original sources. Thus, the half-cell standard potential $E^0 = 0.77$ V vs. SHE is most certainly the correct value. However, as shown in Table 7, there is little agreement on the values for entropy or temperature coefficient, which ranges from 1.1–2 mV K^{-1} [29,32,37,41,42].

The full-cell Fe–V flow battery reaction is obtained by combining Equations (1) and (12):

$$Fe^{3+} + V^{2+} \leftrightarrow Fe^{2+} + V^{3+} \quad (13)$$

Accordingly, the standard thermodynamic quantities can be obtained by subtracting those of the negative side from those of the positive side. The standard thermodynamic values for the full Fe–V cell from various published sources are shown in Table 8. The standard cell potential E^0 varies from 1.02 V to 1.1 V, and reported dE^0/dT values range from −1.04 mV K^{-1} to an estimate of +1 mV K^{-1}. Observed average potentials of Fe–V cells in this and previous studies [14,25,43,44] are significantly lower than the standard potential of 1.02 V. This is likely due to a mixed potential at both electrodes, which occurs because of the presence of both redox species (Fe and V) at both electrodes (i.e. the "mixed reactant" electrolyte composition). Another possible contribution to the deviation from standard potential is the non-unity of activity coefficients arising from high concentration of redox couples and supporting electrolyte species. The one published model of Fe–V flow batteries applied an arbitrary correction factor to the potential to account for the difference [14]. With regard to the temperature coefficient and entropy, there are no known direct measurements of these values for Fe–V cells, and there are no agreed-upon values for the standard entropies of the half-cell reactions. Thus, there is a need for empirical values of thermodynamic quantities (i.e. formal potentials and temperature coefficient) for Fe–V flow batteries, as was argued above for the VRFB.

3.2.2. Nernst Equation with formal potential

The Nernst Equation [16] can be applied to the full-cell Fe–V reaction (Equation (13), where $n = 1$ equiv mol^{-1}) to obtain an expression for cell OCP:

Table 6
Published thermodynamic quantities for the positive electrode reaction of the iron–vanadium and iron–chromium flow batteries. ΔG^0 values are in kJ mol^{-1} and E^0 values are in volts vs. SHE (standard hydrogen electrode).

Source	Year	ΔG_f^0 of Fe^{3+}	ΔG_f^0 of Fe^{2+}	ΔG^0 of half-cell reaction	E^0 of half-cell reaction	Remarks
Latimer book [41]	1952	−10.6	−84.94	−74.4	0.771	Compiled from various references
Pourbaix book [31]	1966	−10.6	−84.9	−74.3	0.770	Compiled from various references
Whittemore and Langmuir [42]	1972	N/A	N/A	−74.3	0.770	Experimentally measured
Wagman et al. tables [37]	1982	−4.7	−78.90	−74	0.77	Comprehensive NBS (NIST) tables
Bard et al. book [29]	1985	−17	−91	−74	0.77	Compiled from various references
Bratsch tables [32]	1989	N/A	N/A	−74.4	0.771	Compiled from various references

Table 7
Published thermodynamic quantities for the positive electrode reaction of the iron–vanadium and iron–chromium flow batteries. S^0 values are in J mol^{-1} K^{-1} and dE^0/dT values are in mV K^{-1}. Values in parentheses are estimated, as stated by the source author(s).

Source	Year	S^0 of Fe^{3+}	S^0 of Fe^{2+}	ΔS^0 of half-cell reaction	dE^0/dT of half-cell reaction	Remarks
Latimer book [41]	1952	−293	−113	180	1.86	Compiled from various references
Whittemore and Langmuir [42]	1972	N/A	N/A	106	1.10	Experimentally measured
Wagman et al. tables [37]	1982	−315.9	−137.7	178.2	1.847	Comprehensive NBS (NIST) tables
Bard et al. book [29]	1985	(−300)	−107	(200)	(2)	Compiled from various references
Bratsch tables [32]	1989	N/A	N/A	113.4	1.175	Compiled from various references

$$E = E^0 + \frac{RT}{F}\ln\left(\frac{a_{V^{2+}} \cdot a_{Fe^{3+}}}{a_{V^{3+}} \cdot a_{Fe^{2+}}}\right) \tag{14}$$

Applying the same strategy as above for the VRFB and given the stoichiometry of Equation (13), the cell OCP can be expressed as a function of formal potential and reactant concentrations (assuming the total amount and concentration of iron species on the positive side equal those of vanadium species on the negative side):

$$E = E^{0\prime} + \frac{2RT}{F}\ln\left(\frac{[V^{2+}]}{[V^{3+}]}\right) \tag{15}$$

Similar to the VRFB, the Fe–V cell has this relationship between state-of-charge and the concentration of the vanadium species: $X = [V^{2+}]/([V^{2+}] + [V^{3+}])$. Thus, the cell OCP can be expressed in terms of X:

$$E = E^{0\prime} + \frac{2RT}{F}\ln\left(\frac{X}{1-X}\right) \tag{16}$$

This relation is simpler than that of the VRFB because the solvated proton is not involved in the reaction. Furthermore, Equation (16) is independent of the concentrations of the active redox species and supporting electrolyte as long as the same discharged solution is used on both sides of the cell (i.e. the mixed-reactant cell). In this case, the formal potential is measured at 50% SOC, where the logarithmic term equals zero. The formal potential in Equation (16) is equal to the average OCP because the integral of the logarithmic term over the range $\{0 \le X \le 1\}$ is equal to zero.

The formal potential $E^{0\prime}$ at 22 °C of the Fe–V chemistry used in this study was determined by measuring cell OCP at 50% SOC as follows. The cell was prepared with equal amounts of mixed $FeCl_2$/VCl_3 (discharged) solution on the positive and negative sides. The cell was fully charged to an upper voltage limit of 1.3 V, which results in an iron oxidation state of +3 on the positive side and a vanadium oxidation state of +2 on the negative side. A 5.0-mL aliquot of "charged" solution was collected on each side, and each of these aliquots was mixed separately with 5.0-mL of the original "discharged" solution. The cell was rinsed by pumping DI water through both sides, and the 10-mL mixtures were pumped through each side to obtain a cell at 50% SOC. The OCP was immediately measured with a digital multimeter, and this value was taken as $E^{0\prime}$. The resultant value was $E^{0\prime} = 0.73$ V, which is the average of two duplicate experiments with a precision of ±0.01 V. This is also the average OCP over the full SOC range.

As shown above for the VRFB, the partial molar Gibbs free energy ($\Delta\overline{G}$) of the Fe–V cell reaction at a particular SOC can be expressed as a function of X and the measured $E^{0\prime}$ value:

$$\Delta\overline{G} = -FE^{0\prime} - 2RT\ln\left(\frac{X}{1-X}\right) \tag{17}$$

The Gibbs free energy of the cell over a full charge or discharge is equal to the integral of $\Delta\overline{G}$ over the range $\{0 \le X \le 1\}$. This calculation is equivalent to taking the average OCP and multiplying it by the Faraday constant or to plugging the value $X = 0.5$ into Equation (17). The result is $\Delta G = -70$ kJ mol^{-1}. As shown in Table 8, this ΔG value differs significantly from previously reported standard values, which should be taken into consideration when selecting thermodynamic values for Fe–V flow battery models.

Use of Equation (16) to calculate the cell potential as a function of formal potential and state-of-charge was verified by comparing the calculated values to measured charge–discharge curves. The calculated potential at 22 °C using $E^{0\prime} = 0.73$ V with Equation (16) is shown in Fig. 4(a) as a function of SOC. This is compared to an experimental charge–discharge curve measured at 50 mA cm^{-2} and 22 °C with a Nafion 117 membrane. The formal potential at 60 °C, $E^{0\prime} = 0.69$ V, was used similarly to calculate an OCP vs. SOC curve and compared to experimental results, as shown in Fig. 4(b). At both temperatures, the calculated OCP curve lies between the charge and discharge curves, but it is significantly closer to the discharge curve. This is especially true at 60 °C, where a significant portion of the calculated OCP curve overlaps with the measured discharge. This may be because the cell is in a mixed-reactant configuration, with the effect of mixed potential being more pronounced when the cell is sitting at open circuit. Another proposed explanation for this is that the kinetics at one or both electrodes are significantly faster for the discharge reactions than for the charge reactions. This possibility should be taken into consideration as models of Fe–V flow batteries are developed further. If either proposed explanation is true, then the results in Fig. 4 show that the Nernst Equation, expressed as Equation (16), is a valid expression for relating cell OCP and SOC.

Table 8
Thermodynamic quantities for the iron–vanadium cell reaction. Values in parentheses are estimated, as stated by the source author(s).

Source	Year	ΔG of cell reaction (kJ mol^{-1})	E of cell (V)	ΔS of cell reaction (J mol^{-1} K^{-1})	dE/dT of cell (mV K^{-1})	Remarks
Pourbaix book [31]	1966	−98.9	1.02	N/A	N/A	Standard values
Bard et al. book [29]	1985	−110	1.1	(100)	(1)	Standard values
Bratsch tables [32]	1989	−99.0	1.03	(−31)	(−0.32)	Standard values
This work	2013	−70	0.73	−100	−1.04	Formal potential (22 °C) and dE/dT (22–80 °C) measured at 50% SOC

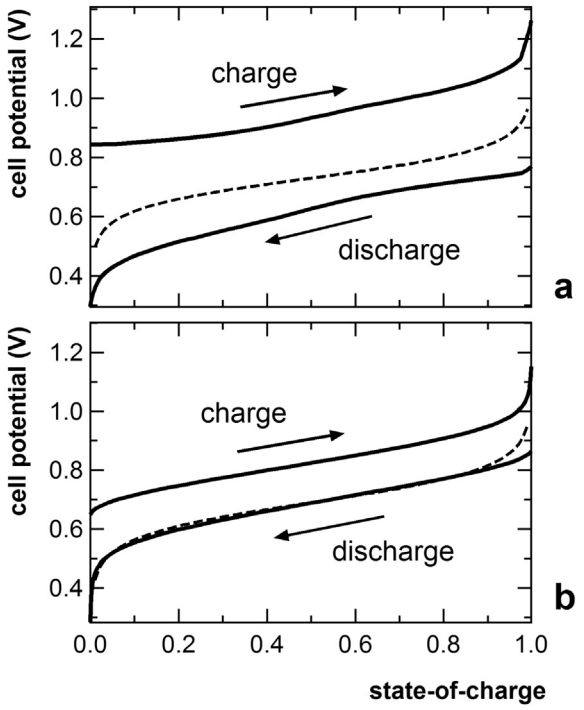

Fig. 4. Measured galvanostatic charge–discharge potential (solid lines) compared to calculated OCP (dashed lines) for the Fe–V flow battery. (a) 22 °C, at which $E^{0\prime} = 0.73$ V. (b) 60 °C, at which $E^{0\prime} = 0.69$ V. SOC was calculated as in Fig. 2. OCP was calculated using the Nernst Equation (Equation (16)) with the measured formal potential $E^{0\prime}$.

3.2.3. Temperature coefficient and entropy values

An expression for the temperature coefficient dE/dT of the Fe–V cell can be obtained by taking the derivative of Equation (16) with respect to temperature:

$$\frac{dE}{dT} = \frac{dE^{0\prime}}{dT} + \frac{2R}{F}\ln\left(\frac{X}{1-X}\right) \tag{18}$$

where dE/dT is in units of volts K^{-1}. In this case, the formal temperature coefficient ($dE^{0\prime}/dT$) is measured at $X = 0.50$, and a constant value was observed over the range 22–80 °C. This experiment was performed in duplicate with two separately prepared cells, and the average of the two measurements was $dE^{0\prime}/dT = -1.04 \pm 0.03$ mV K^{-1}. This value is also the average dE/dT value over the full range of state-of-charge.

As shown above for the VRFB, the partial molar entropy of the Fe–V cell reaction ($\Delta\bar{S}$) as a function of SOC can be expressed as:

$$\Delta\bar{S} = F\frac{dE^{0\prime}}{dT} + 2R\ln\left(\frac{X}{1-X}\right) \tag{19}$$

The entropy of the cell over a full charge or discharge is equal to the integral of $\Delta\bar{S}$ over the range $\{0 \le X \le 1\}$. This calculation is equivalent to multiplying the formal temperature coefficient $dE^{0\prime}/dT$ or average temperature coefficient in V K^{-1} by the Faraday constant, which gives $\Delta S = -100$ J mol^{-1} K^{-1}. As shown in Table 8, the dE/dT and entropy values measured here are significantly different from the estimated values given in the literature [29,32].

In order to confirm the validity of the relation between temperature coefficient and SOC in Equation (18), dE/dT values were measured in Fe–V cells at various states-of-charge. The SOC was varied by charging or discharging a cell for an arbitrary amount of time. The state-of-charge in each case was obtained by using the measured OCP at 22 °C in Equation (16) and solving for X. The measured data were compared to the dE/dT vs. X curve calculated using $dE^{0\prime}/dT = -1.04$ mV K^{-1} with Equation (18). The comparison is shown in Fig. 5, in which there is good agreement between measured and calculated values. This proves that the derivative of the Nernst Equation, as expressed in Equation (18), is valid for Fe–V flow batteries. Fig. 5 also shows good repeatability of the measurements, as the data were gathered from five separately prepared cells.

Because the Nernst Equation has been validated above for relating state-of-charge, cell potential, and temperature coefficient in the Fe–V flow battery, a combined expression for calculating cell OCP as a function of temperature and SOC (X) can be used for the given temperature range 22–80 °C:

$$E(T,X) = E^{0\prime}\big|_{22\,^\circ C} + (T - 295\ K)\frac{dE^{0\prime}}{dT} + \frac{2RT}{F}\ln\left(\frac{X}{1-X}\right) \tag{20}$$

3.3. Iron–chromium (Fe–Cr) cells

3.3.1. Cell reactions and published thermodynamic data

The half-cell reaction on the negative electrode side of the Fe–Cr flow battery is:

$$Cr^{2+} + e^- \leftrightarrow Cr^{3+} \tag{21}$$

Table 9 contains the standard Gibbs free energy of formation (ΔG_f^0) for these two oxidation states of chromium in aqueous solution, culled from three publications [29,32,41]. The ΔG^0 and E^0 of the half-cell reaction calculated from these values are also given in Table 9. There is general agreement among the values for the half-cell reaction, all of which give a half-cell standard potential of about $E^0 = -0.4$ V vs. SHE. As shown in Table 10, there are no generally accepted values for dE/dT or ΔS^0, only two estimated values that are not in agreement [29,32].

The half-cell reaction on the positive side of the Fe–Cr flow battery is the same as that of the Fe–V flow battery, given in Equation (12) above. The full-cell Fe–Cr flow battery reaction is obtained by combining Equations (12) and (21):

$$Fe^{3+} + Cr^{2+} \leftrightarrow Fe^{2+} + Cr^{3+} \tag{22}$$

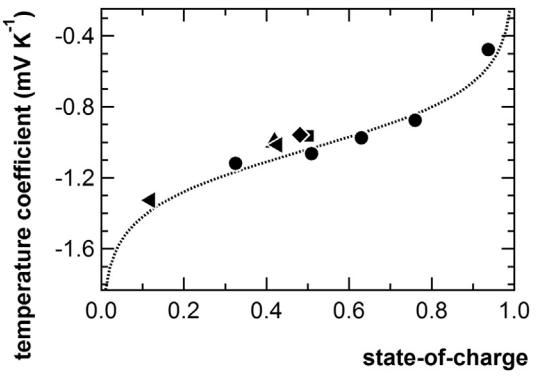

Fig. 5. Measured dE/dT (markers) compared to calculated dE/dT (line) as a function of state-of-charge X for the Fe–V flow battery. The calculation was performed using Equation (18) (temperature derivative of the Nernst Equation) and the formal temperature coefficient, $dE^{0\prime}/dT = -1.04$ mV K^{-1}. The X value for each experimental dE/dT point was calculated using Equation (16) with the measured OCP at 22 °C and the formal potential at 22 °C ($E^{0\prime} = 0.73$ V). Different marker shapes correspond to separately prepared cells. Nafion 117 was used as the membrane. There are 10 data points total, taken from 5 separately prepared cells.

Table 9
Published thermodynamic quantities for the negative electrode reaction of the iron–chromium flow battery. ΔG^0 values are in kJ mol^{-1} and E^0 values are in volts vs. SHE (standard hydrogen electrode). Values in each reference were compiled from various sources.

Source	Year	ΔG_f^0 of Cr^{3+}	ΔG_f^0 of Cr^{2+}	ΔG^0 of half-cell reaction	E^0 of half-cell reaction
Latimer book [41]	1952	−215	−176	39.3	−0.407
Bard et al. book [29]	1985	−215	−174	41.0	−0.424
Bratsch tables [32]	1989	N/A	N/A	40	−0.42

Table 10
Published thermodynamic quantities for the negative electrode reaction of the iron–chromium flow battery. S^0 values are in J mol^{-1} K^{-1} and dE^0/dT values are in mV K^{-1}. Values in parentheses are estimated, as stated by the source author(s). Values in each reference were compiled from various sources.

Source	Year	S^0 of Cr^{3+}	S^0 of Cr^{2+}	ΔS^0 of half-cell reaction	dE^0/dT of half-cell reaction
Latimer book [41]	1952	−308	N/A	N/A	N/A
Bard et al. book [29]	1985	(−293)	(−100)	(193)	(2.00)
Bratsch tables [32]	1989	N/A	N/A	(140)	(1.4)

This cell reaction is similar to the Fe–V flow cell reaction in Equation (13). The standard thermodynamic values for the full Fe–Cr cell from three published sources are shown in Table 11. The standard cell potential E^0 is generally agreed to be 1.2 V, and estimated dE^0/dT values are +0.07 mV K^{-1} [29] or −0.22 mV K^{-1} [32]. Observed average potentials of Fe–Cr cells in this and previous studies are significantly lower than the standard potential. As stated above for the Fe–V mixed reactant cell, this is likely due to the mixed potentials at both electrodes or to the non-unity of $Fe^{3+/2+}$ and $Cr^{2+/3+}$ activity coefficients. Previous studies have reported [45] or made use of [15] formal potentials of Fe–Cr cells, but there are no known direct measurements of dE/dT or ΔS for this type of cell.

3.2.2. Formal potential and free energy values

The Nernst Equation [16] can be applied to the full-cell Fe–Cr reaction (Equation (22), where $n = 1$ equiv mol^{-1}) to obtain an expression that is identical to Equation (14) except with chromium species activities in place of vanadium species activities. Similarly, Equation (15) applies to the Fe–Cr cell with chromium species concentrations in place of vanadium species concentrations. The state-of-charge X in the Fe–Cr cell is calculated by the relation $X = [Cr^{2+}]/([Cr^{2+}] + [Cr^{3+}])$, so Equations (16) and (17) also apply to the Fe–Cr cell for relating E and $\Delta\overline{G}$, respectively, to the state-of-charge X. The formal potential $E^{0\prime}$ is equivalent to the average potential and is measured at 50% SOC.

The formal potential $E^{0\prime}$ at 22 °C of the Fe–Cr chemistry used in this study was determined by measuring cell OCP at 50% in a manner similar to that described above for Fe–V cells. In the case of the Fe–Cr cells, the initial charge step was conducted at 50 mA cm^{-2} and 10 mA cm^{-2} to an upper voltage limit of 2.0 V. Lower current densities were required because of the absence of a catalyst at the negative electrode. In practical Fe–Cr cells, a catalyst is always required at the negative (chromium-active) side of the cell to avoid prohibitively large overpotentials [26]. The average of duplicate OCP measurements at 50% SOC resulted in $E^{0\prime} = 0.98 \pm 0.01$ V. This value can be used in Equations (16) and (17) for this particular Fe–Cr flow battery composition. It is also the average OCP over the full SOC range. The corresponding ΔG over the full SOC range is −95 kJ mol^{-1}. As shown in Table 11, this value differs significantly from previously reported standard values, which should be taken into consideration when selecting thermodynamic values for Fe–Cr flow battery models. Because of the absence of a catalyst at the negative electrode, charge–discharge cycling was not performed on the Fe–Cr cell in this study. However, the thermodynamic quantities measured here should be applicable whether or not a catalyst is present given that the catalyst provides only a kinetic effect on flow battery performance (i.e. does not theoretically affect the measurement of OCP, or *equilibrium* potential).

3.3.3. Temperature coefficient and entropy values

The expression for dE/dT of the Fe–Cr cell is identical to that of the Fe–V cell, Equation (18), because the electrode reactions and stoichiometry are the same. The expression for partial-molar entropy, Equation (19), is also the same. The formal temperature coefficient of the Fe–Cr cell was measured at $X = 0.50$, and a constant value of $dE^{0\prime}/dT = -0.68$ mV K^{-1} was observed over the range 22–40 °C. At higher temperature, the decrease in cell potential over time due to self-discharge was too extreme to obtain reliable dE/dT measurements. This was also the case when Nafion 117 was used as the membrane at any temperature, so all dE/dT measurements were performed with Neosepta AMX membranes. The corresponding ΔS over the full SOC range is −66 J mol^{-1} K^{-1}. This provides a more concrete entropy value than previously published, estimated values.

In order to confirm the validity of Equation (18) for Fe–Cr cells, dE/dT values were measured over the range 22–40 °C at various states-of-charge. The SOC was varied by charging or discharging a cell for an arbitrary amount of time. The state-of-charge in each case was obtained by using the measured OCP at 22 °C in Equation (16) and solving for X. The measured data were compared to the dE/dT vs. X curve calculated using $dE^{0\prime}/dT = -0.68$ mV K^{-1} with Equation (18). The comparison is shown in Fig. 6, in which there is good agreement between measured and calculated values. This proves that the derivative of the Nernst Equation, as expressed in Equation (18), is valid for Fe–Cr flow batteries. Fig. 6 also shows

Table 11
Thermodynamic quantities for the iron–chromium cell reaction. Values in parentheses are estimated, as stated by the source author(s).

Source	Year	ΔG of cell reaction	E of cell	ΔS of cell reaction	dE/dT of cell	Remarks
Latimer book [41]	1952	−114	1.18	N/A	N/A	Standard values
Bard et al. book [29]	1985	−120	1.2	(7)	(0.07)	Standard values
Bratsch tables [32]	1989	−120	1.2	(−22)	(−0.22)	Standard values
Gahn et al. report [45]	1983	−86	0.89	N/A	N/A	Formal potential of mixed-reactant cell measured at 65 °C and 50% SOC
This work	2013	−95	0.98	−66	−0.68	Formal potential (22 °C) and dE/dT (22–40 °C) measured at 50% SOC

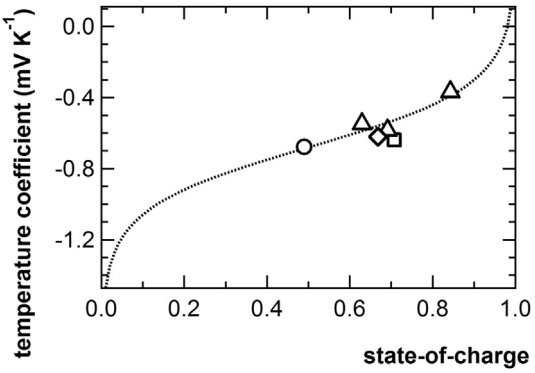

Fig. 6. Measured dE/dT (markers) compared to calculated dE/dT (line) as a function of state-of-charge X for the Fe–Cr flow battery. The calculation was performed using Equation (18) (temperature derivative of the Nernst Equation) and the formal temperature coefficient, $dE^{0\prime}/dT = -0.68$ mV K^{-1}. The X value for each experimental dE/dT point was calculated using Equation (16) with the measured OCP at 22 °C and the formal potential at 22 °C ($E^{0\prime} = 0.98$ V). Different marker shapes correspond to separately prepared cells. Neosepta AMX was used as the membrane. There are 6 data points total, taken from 4 separately prepared cells.

good repeatability of the measurements, as the data were gathered from four separately prepared cells. Thus, Equation (20) is also a valid expression for the OCP of the Fe–Cr cells as a function of temperature and state-of-charge over the range 22–40 °C.

3.4. Non-isothermal cycling of flow batteries

The thermodynamic quantities provided herein are not only useful for thermo-electrochemical flow battery models but also in the design of flow battery systems, specifically with regard to the selection of operating temperature(s). In some cases, it may be beneficial to operate charge and discharge portions of the battery cycle at different temperatures in order to minimize voltage during charge and maximize voltage during discharge. As demonstrated here, the state-of-the-art flow battery chemistries based on aqueous iron and vanadium solutions all have cell temperature coefficients that are negative. Thus, higher temperature corresponds to lower cell potential. This is evident in Fig. 7(a), which gives the calculated OCP curves for the VRFB at 22 °C and 60 °C. If the battery is charged at higher temperature and discharged at lower temperature, its voltage efficiency ($E_{discharge}/E_{charge}$) may be higher than that of a cell that is cycled isothermally at either temperature. This effect will be more pronounced when the magnitude of dE/dT is higher.

The experimental cycling data for VRFB and Fe–V cells at 22 °C and 60 °C were used to test the hypothesis of improved voltage efficiency through non-isothermal cycling. Fig. 7(b) shows the galvanostatic charge and discharge curves of the VRFB at 50 mA cm^{-2}. As expected, the voltage gap between charge and discharge is lower at the higher temperature because voltage losses from ohmic, kinetic, and transport effects are lower. However, the lower equilibrium potential at 60 °C results in discharge potentials that are mostly lower than those at 22 °C. Thus, there is an advantage to discharging the cell at 22 °C because the higher voltage corresponds to higher energy and power output. Table 12 shows the voltage efficiencies (calculated here as the average discharge potential divided by the average charge potential) for isothermal and non-isothermal cycling. When the current density is 50 mA cm^{-2}, the isothermal voltage efficiency is 3.9% higher at 60 °C relative to 22 °C. When the voltage efficiency calculation is performed using the charge potential at 60 °C and the discharge

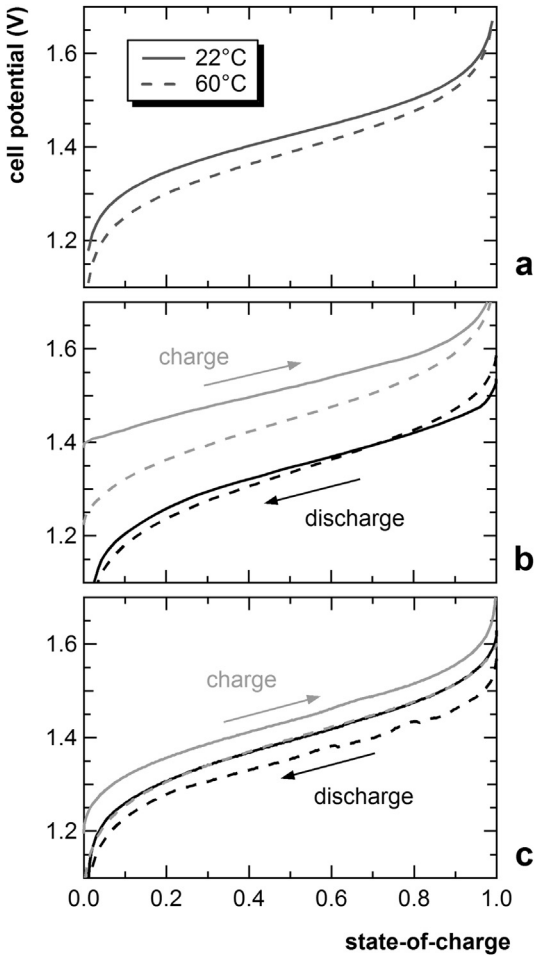

Fig. 7. Charge, discharge, and open-circuit potentials of VRFB as a function of SOC at two temperatures. (a) Calculated OCP. (b) Galvanostatic charge–discharge potentials measured at 50 mA cm^{-2}. (c) Galvanostatic charge–discharge potentials measured at 10 mA cm^{-2}. OCP and SOC calculated as in Fig. 2.

potential at 22 °C, the result is an additional 0.3% higher. The effect is even more pronounced at lower current densities, where voltage losses are less significant. As shown in Fig. 7(c), the charge curve at 10 mA cm^{-2} and 60 °C is almost completely superimposed on the discharge curve at 10 mA cm^{-2} and 22 °C. Accordingly, the voltage efficiency when operating in non-isothermal mode at this current density is 99.8%. This is significantly higher than the isothermal voltage efficiency at either temperature, as shown in Table 12.

In contrast to the VRFB, non-isothermal cycling of the Fe–V cell at 50 mA cm^{-2} was disadvantageous. The galvanostatic cycling curves for both temperatures are shown in Fig. 8. In this cell, the voltage losses are more significant than in the VRFB, which results in wider voltage gaps and lower voltage efficiencies at both

Table 12
Voltage efficiency of VRFB and Fe–V cells under isothermal and non-isothermal cycling. Values were calculated from galvanostatic charge and discharge curves measured at 22 °C and 60 °C.

Temperature configuration	VRFB at 10 mA cm^{-2}	VRFB at 50 mA cm^{-2}	Fe–V at 50 mA cm^{-2}
Isothermal at 22 °C	96.4%	87.5%	64.4%
Isothermal at 60 °C	97.0%	91.4%	82.2%
Charge at 60 °C, discharge at 22 °C	99.8%	91.7%	73.6%

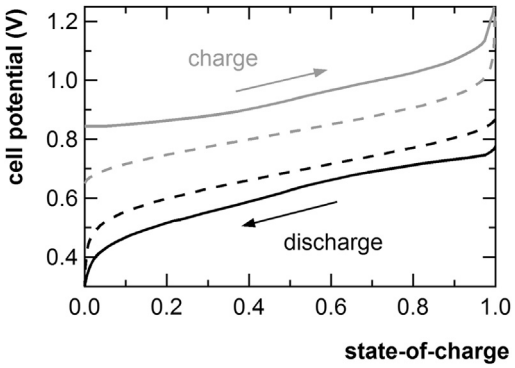

Fig. 8. Galvanostatic charge and discharge potentials of Fe–V flow cell at 22 °C (solid line) and 60 °C (dashed line). SOC calculated as in Fig. 2.

temperatures. The overall potential at 60 °C is lower than that at 22 °C because of the negative dE/dT, but this is outweighed by the high voltage losses. Thus, the discharge curve at 60 °C is higher in potential than that at 22 °C, and isothermal cycling at 60 °C results in the highest voltage efficiency, as shown in Table 12. However, the voltage efficiency of the Fe–V cell at room temperature presented here is significantly lower than that of previously demonstrated Fe–V cells [25]. In an optimized system, the voltage losses could be minimized enough so that non-isothermal operation provides an efficiency advantage. While the thermodynamics (E and dE/dT) of a particular flow battery chemistry provide an initial indication of this non-isothermal advantage, the kinetics of the system in question will ultimately determine whether and to what extent the advantage exists.

Actual implementation of non-isothermal cycling at the system level can be envisioned in several ways. In cases where electrical energy is expended to heat a flow battery stack to particular temperature, the electrical heat source may be turned off when the cells are in discharge mode, allowing the stack to cool towards room temperature. This will not only provide the increase in voltage efficiency described above but also may result in an increase to the overall energy efficiency of the system by using less parasitic heating energy. In other cases, waste heat from processes external to the battery (e.g. hot effluents from power plant processes) may be used to bring the battery to an operating temperature above ambient. During the charge portion of each cycle, the flow battery reactants can be passed through a heat exchanger in contact with the external heat source before entering the cell stack. During the discharge portion of the cycle, the reactants can be re-routed with valves to bypass the heat exchanger and enter the stack at ambient temperature. In either case (added parasitic heating energy or harvested waste heat), non-isothermal cycling may be implemented by utilizing two separate cell stacks, one for charging and the other for discharging, each of which is maintained at a different temperature. In this implementation, the flow battery reactants would be automatically routed to either stack according to whether the battery is being charged or discharged. In any case, the extent of the advantage of non-isothermal cycling will be dependent on the battery chemistry and on the specific design of the cells, stacks, and system. Extensive modeling and design of a particular system will be necessary to determine the feasibility of using a non-isothermal operation mode. Furthermore, the effects of large and repeated changes in temperature to flow battery solutions are largely unknown and may result in precipitation or undesired side reactions, which would be prohibitive in the implementation of the non-isothermal cycling strategy.

4. Conclusions

A simple method can be used, as demonstrated here, to experimentally determine thermodynamic quantities, including equilibrium cell potential, temperature coefficient (dE/dT), Gibbs free energy, and entropy, for flow batteries. Such quantities will be useful in thermo-electrochemical models of flow batteries at the cell or system level. A review of previously published, *standard* thermodynamic quantities for aqueous vanadium- and iron-based flow batteries shows that unverified and varied values have often been reported. This is especially true for the dE/dT and entropy values of flow battery electrode reactions, for which there has been no consensus and little experimental evidence. In many cases, these unverified standard values have been used in flow battery models even though typical flow battery conditions are far from standard.

Proof was given herein that formal potentials and formal temperature coefficients can be used with modified forms of the Nernst Equation to quantify the thermodynamics of flow cell reactions as a function of state-of-charge. Complete expressions for cell potential as a function of temperature and state-of-charge were also given. Formal potentials and temperature coefficients are measured for specific flow battery compositions, and values were given above for all-vanadium, iron–vanadium, and iron–chromium flow cells with state-of-the-art solution compositions. Temperature coefficients at a given state-of-charge were shown to be constant over a given temperature range. In other words, a linear relationship between cell potential and temperature was observed. In most cases, the measured thermodynamic quantities were significantly different than those reported and used previously in the literature. The thermodynamic quantities reported herein are for full cell reactions and can only be used as such in thermo-electrochemical models. For models that treat the thermodynamics of positive and negative electrode reactions separately, further experiments to measure formal potential and dE/dT of half-cell reactions against the standard hydrogen electrode may be necessary. In some cases, the full-cell thermodynamic quantities may be used with previously published, standard half-cell quantities to estimate the values for the other half-cell of a given flow battery chemistry.

The thermodynamic values given here, specifically the partial derivative of cell potential with respect to temperature (dE/dT), are also useful in the selection of operating temperatures for flow battery systems. Because the equilibrium potential of a cell reaction is dependent on temperature, it is sometimes beneficial to charge the cell at a temperature corresponding to lower potential and discharge the cell a temperature corresponding to higher potential. This can result in higher voltage efficiency relative to that of an isothermal system at low or high temperature. Proof-of-concept of improved voltage efficiency with such non-isothermal cycling was given above for the all-vanadium redox flow battery, and the effect was more pronounced at lower current densities. This strategy may be useful in scaled-up flow battery systems to improve round-trip energy efficiency, especially when waste heat is available for raising the temperature of cell stacks. The feasibility and benefits of such an approach would be highly dependent on the thermodynamics, kinetics, and operating conditions of a specific flow battery system.

Acknowledgments

The author gratefully acknowledges the financial support of the U.S. Department of Energy's Office of Electricity Delivery and Energy Reliability (Dr. Imre Gyuk, Energy Storage Program Manager). The author also thanks David Ingersoll and Karen Waldrip, both of Sandia National Laboratories, for helpful discussions and ideas. Sandia National Laboratories is a multi-program laboratory

managed and operated by Sandia Corporation, a wholly owned subsidiary of Lockheed Martin Corporation, for the U.S. Department of Energy's National Nuclear Security Administration under contract DE-AC04-94AL85000.

References

[1] B. Dunn, H. Kamath, J.-M. Tarascon, Science 334 (2011) 928–935.
[2] Z. Yang, J. Zhang, M.C.W. Kintner-Meyer, X. Lu, D. Choi, J.P. Lemmon, J. Liu, Chem. Rev. 111 (2011) 3577–3613.
[3] C. Ponce de León, A. Frías-Ferrer, J. González-García, D.A. Szánto, F.C. Walsh, J. Power Sources 160 (2006) 716–732.
[4] M. Skyllas-Kazacos, M.H. Chakrabarti, S.A. Hajimolana, F.S. Mjalli, M. Saleem, J. Electrochem. Soc. 158 (2011) R55–R79.
[5] W. Wang, Q. Luo, B. Li, X. Wei, L. Li, Z. Yang, Adv. Funct. Mater. 23 (2013) 970–986.
[6] H. Al-Fetlawi, A.A. Shah, F.C. Walsh, Electrochim. Acta 55 (2009) 78–89.
[7] H. Al-Fetlawi, A.A. Shah, F.C. Walsh, Electrochim. Acta 55 (2010) 3192–3205.
[8] G. Qiu, A.S. Joshi, C.R. Dennison, K.W. Knehr, E.C. Kumbur, Y. Sun, Electrochim. Acta 64 (2012) 46–64.
[9] A.A. Shah, M.J. Watt-Smith, F.C. Walsh, Electrochim. Acta 53 (2008) 8087–8100.
[10] M. Vynnycky, Energy 36 (2011) 2242–2256.
[11] M.J. Watt-Smith, P. Ridley, R.G.A. Wills, A.A. Shah, F.C. Walsh, J. Chem. Technol. Biotechnol. 88 (2013) 126–138.
[12] D. You, H. Zhang, J. Chen, Electrochim. Acta 54 (2009) 6827–6836.
[13] A.A. Shah, H. Al-Fetlawi, F.C. Walsh, Electrochim. Acta 55 (2010) 1125–1139.
[14] D. Stephenson, S. Kim, F. Chen, E. Thomsen, V. Viswanathan, W. Wang, V. Sprenkle, J. Electrochem. Soc. 159 (2012) A1993–A2000.
[15] P.S. Fedkiw, R.W. Watts, J. Electrochem. Soc. 131 (1984) 701–709.
[16] A.J. Bard, L.R. Faulkner, Electrochemical Methods: Fundamentals and Applications, second ed., Wiley, New York, 2001.
[17] D. Bernardi, E. Pawlikowski, J. Newman, J. Electrochem. Soc. 132 (1985) 5–12.
[18] W.B. Gu, C.Y. Wang, J. Electrochem. Soc. 147 (2000) 2910–2922.
[19] A.J. deBethune, T.S. Licht, N. Swendeman, J. Electrochem. Soc. 106 (1959) 616–625.
[20] J.O. Hill, I.G. Worsley, L.G. Hepler, Chem. Rev. 71 (1971) 127–137.
[21] A. Heintz, C. Illenberger, Ber. Bunsen Phys. Chem. 102 (1998) 1401–1409.
[22] T. Sukkar, M. Skyllas-Kazacos, J. Membr. Sci. 222 (2003) 235–247.
[23] K.W. Knehr, E.C. Kumbur, Electrochem. Commun. 13 (2011) 342–345.
[24] L. Li, S. Kim, W. Wang, M. Vijayakumar, Z. Nie, B. Chen, J. Zhang, G. Xia, J. Hu, G. Graff, J. Liu, Z. Yang, Adv. Energy Mater. 1 (2011) 394–400.
[25] W. Wang, S. Kim, B. Chen, Z. Nie, J. Zhang, G.-G. Xia, L. Li, Z. Yang, Energy Environ. Sci. 4 (2011) 4068–4073.
[26] M. Lopez-Atalaya, G. Codina, J.R. Perez, J.L. Vazquez, A. Aldaz, J. Power Sources 39 (1992) 147–154.
[27] S. Kim, J. Yan, B. Schwenzer, J. Zhang, L. Li, J. Liu, Z. Yang, M.A. Hickner, Electrochem. Commun. 12 (2010) 1650–1653.
[28] K.J. Kim, Y.-J. Kim, J.-H. Kim, M.-S. Park, Mater. Chem. Phys. 131 (2011) 547–553.
[29] A.J. Bard, R. Parsons, J. Jordan, Standard Potentials in Aqueous Solution, first ed., M. Dekker, New York, 1985.
[30] K. Post, R.G. Robins, Electrochim. Acta 21 (1976) 401–405.
[31] M. Pourbaix, Atlas of Electrochemical Equilibria in Aqueous Solutions, first English ed., Pergamon Press, Oxford, New York, 1966.
[32] S.G. Bratsch, J. Phys. Chem. Ref. Data 18 (1989) 1–21.
[33] G. Jones, J.H. Colvin, J. Am. Chem. Soc. 66 (1944) 1573–1579.
[34] J.E. Carpenter, J. Am. Chem. Soc. 56 (1934) 1847–1850.
[35] C.D. Coryell, D.M. Yost, J. Am. Chem. Soc. 55 (1933) 1909–1915.
[36] M.J. LaSalle, J.W. Cobble, J. Phys. Chem. 59 (1955) 519–524.
[37] D.D. Wagman, W.H. Evans, V.B. Parker, R.H. Schumm, I. Halow, S.M. Bailey, K.L. Churney, R.L. Nuttall, J. Phys. Chem. Ref. Data 11 (suppl. 2) (1982), 2-1–2-392.
[38] J.A. Dean, N.A. Lange, Lange's Handbook of Chemistry, McGraw-Hill, New York, 1973.
[39] J.R. Dahn, R.R. Haering, Can. J. Phys. 61 (1983) 1093–1098.
[40] A. Honders, J.M. der Kinderen, A.H. van Heeren, J.H.W. de Wit, G.H.J. Broers, Solid State Ionics 14 (1984) 205–216.
[41] W.M. Latimer, The Oxidation States of the Elements and Their Potentials in Aqueous Solutions, second ed., Prentice-Hall, New York, 1952.
[42] D.O. Whittemore, D. Langmuir, J. Chem. Eng. Data 17 (1972) 288–290.
[43] B. Li, L. Li, W. Wang, Z. Nie, B. Chen, X. Wei, Q. Luo, Z. Yang, V. Sprenkle, J. Power Sources 229 (2013) 1–5.
[44] W. Wang, Z. Nie, B. Chen, F. Chen, Q. Luo, X. Wei, G.-G. Xia, M. Skyllas-Kazacos, L. Li, Z. Yang, Adv. Energy Mater. 2 (2012) 487–493.
[45] R.F. Gahn, N.H. Hagedorn, J.S. Ling, NASA Technical Memos, NASA-TM-83385, 1983.